CHEMISTRY OF MATERIALS

pubs.acs.org/cm

Article

High-Silica, Enantiomerically Enriched STW-Type Molecular Sieves

Youngkyu Park, Faisal H. Alshafei, Lygia Silva De Moraes, Isabel Hernandez Rodriguez, Michael W. Deem, Hosea M. Nelson, and Mark E. Davis*

Cite This: https://doi.org/10.1021/acs.chemmater.4c01792

Read Online

ACCESS | Metrics & More | Article Recommendations | Supporting Information

ABSTRACT: Enantiomerically enriched molecular sieves can provide new opportunities for enantioselective catalysis and adsorption. The potential of using these materials for practical applications relies on the preparation of stable materials that can survive the rigors of use and regeneration. Reported enantiomerically enriched STW-type molecular sieves contain large amounts of Ge that limit the structural stability. Higher Si-containing STW-type molecular sieves will have enhanced stability, which should enable practical application. To achieve high-silica framework composition within enantiomerically enriched STW-type molecular sieves, a chiral organic structure-directing agent (OSDA) is computationally designed based on predicted stabilization energy toward the STW framework that is superior to previously employed OSDAs. With enantiopure forms of the designed OSDA, the synthesis of enantiomerically enriched STW-type germanosilicate molecular sieves with the framework Si/Ge as high as 18 is achieved. This high-silica STW-type molecular sieve has a significantly higher Si framework composition from the previously reported enantiomerically enriched germanium-rich STW-type molecular sieve and exhibits stability upon thermal treatment to 800 °C. The absolute stereochemistry of the framework structure is characterized by the dynamical refinement of microcrystal electron diffraction data from several microcrystals. The enantioselective adsorption of 2-butanol is demonstrated over the high-silica, enantioenriched STW-type molecular sieve.

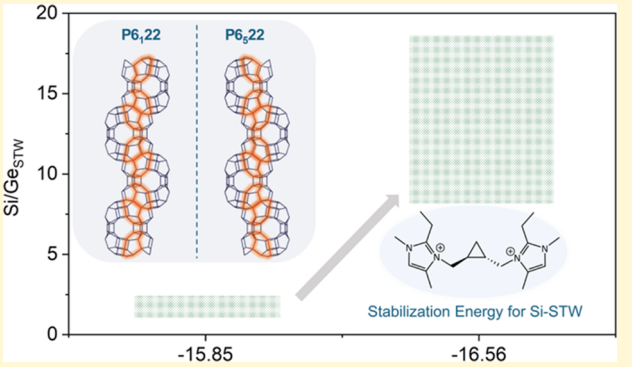

1. INTRODUCTION

The production of enantiomerically pure compounds has significant industrial relevance, as the opposite enantiomers often show different biological activities.[1−4] Materials that function as enantioselective catalysts and adsorbents are useful to obtain the enantiomeric enrichment of target products.[5−7] Since molecular sieves, crystalline microporous materials based on tetrahedrally coordinated oxide (TO_4, T denotes a tetrahedrally coordinated atom) units, including aluminosilicate zeolites and silicoaluminophosphtes, are widely used in many applications of adsorption and catalysis, there have been continued efforts to achieve enantioselectivity over these types of solids.[8−12] The well-defined channel systems with the subnanometer scale enable the molecular sieves to exhibit shape-selective adsorption and catalysis, and the chemistry of the substrate molecules strongly depends on the framework topology. Hence, the preparation of molecular sieves with chiral framework topology has been the primary goal to achieve enantioselective catalysis and adsorption.[13]

The first synthesis of enantiomerically enriched molecular sieves was reported in 2017 by Brand et al., where the STW-type molecular sieves (the framework structures of molecular sieves are assigned distinct three-letter codes) were prepared using enantiopure diquaternary organic structure-directing agents (OSDAs).[14] Among several inherently chiral framework topologies such as *BEA (intergrowth family Beta), GOO, -ITV, and JRY ("-" indicates the interrupted structure with T atoms that are not connected to four neighboring T atoms[15]), the STW-type framework exhibits structural chirality based on its 6-fold helical rotation of the 10-membered ring (10 MR, the pore composed of 10 connected TO_4 units) channel along the *c*-axis. Depending on the direction of the helical rotation of the 10 MR channel, the two enantiomers crystallize in the $P6_122$ and $P6_522$ space groups (Figure 1). The STW-type framework is not an intergrowth structure of different polymorphs such as zeolite Beta, and each STW crystal grows as a single enantiomorph. Since the two enantiomorphs of the STW framework with the same chemical composition would have the same energy, it is essential to use enantiopure OSDAs that can energetically distinguish the two enantiomorphs of STW and favor the crystallization of a specific enantiomorph over the opposite. Brand et al. designed a chiral OSDA with the aid of computational predictions of stabilization energy toward the

Received: June 28, 2024
Revised: October 3, 2024
Accepted: October 4, 2024

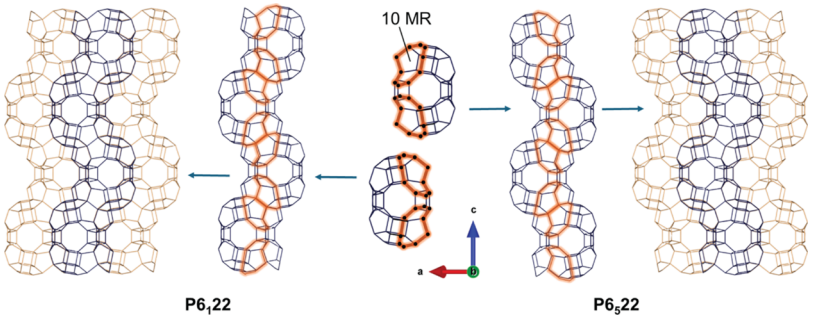

Figure 1. Helical rotation of the 10 MR channel within the STW framework topology with $P6_122$ and $P6_522$ space groups.

STW-type framework structure, and the STW-type molecular sieves prepared by these enantiopure OSDAs showed chiral functionality in the adsorption of 2-butanol and the epoxide ring opening reactions.[14]

Recently, de la Serna et al. reported the synthesis of other enantioenriched molecular sieves with -ITV-type framework topology, GTM-3 and GTM-4.[16−18] The -ITV structure also exhibits linear chirality based on the 4-fold helical rotation of the pore along the *c*-axis, generating frameworks with the two possible space groups, namely, $P4_122$ and $P4_322$. The interrupted nature of the -ITV framework structure that contains a significant amount of T−OH due to the unconnected T−O−T bond provides an extra-large pore 30 MR channel. These materials were prepared using various derivatives of enantiopure (pseudo)ephedrine-based OSDAs and showed improved enantioselectivity toward the ring-aperture reactions of bulky epoxides such as stilbene oxide.

While these successful syntheses proved the promise of chiral molecular sieves as enantioselective catalysts and adsorbents, improving the framework stability of these materials remains a primary goal to achieve. The reported enantioenriched molecular sieves are mainly composed of d4r (double four-ring) units that are favorably built in the presence of fluoride (F) ion and germanium (Ge) in the synthesis gel. In particular, the high Ge content within the framework was unavoidable in both STW- and -ITV-type molecular sieves with enantioenrichment. While the addition of Ge provides better structural flexibility to form various framework topologies, it reduces the stability of the framework structure, as the Ge−O−Si(Ge) bond is easily hydrolyzed and forms Ge−OH and HO−Si(Ge). Thus, Ge-rich germanosilicate molecular sieves are often susceptible to the loss of crystallinity upon the removal of pore-filling OSDAs. Therefore, it is desired to decrease the Ge content in the framework and improve the structural stability.

Here, we present the synthesis of enantiomerically enriched high-silica STW-type molecular sieves using a new chiral OSDA. The OSDA is designed by use of predicted stabilization energy toward the STW framework and prepared via a new synthesis route. The high-silica enantioenriched STW-type molecular sieve exhibits the desired improved framework stability upon the removal of OSDA by thermal treatment.

2. METHODS

2.1. Computation of Stabilization Energy. Calculation of the predicted stabilization energy of diquats was implemented following the previously published method.[14,19,21] A total of 84 chiral diquaternary (CDQ) structures were generated by the combination of the cyclopropane-based chiral linker and imidazole moieties with varied alkyl branches. The stabilization energies of enantiomers with (1*S*,2*S*) configuration (*S*-CDQ) were computed by the optimal geometric placement of three *S*-CDQ molecules within a unit cell of the STW framework, energy minimization, and finally a molecular dynamics run at 343 K to compute the average stabilization energy. This procedure was repeated 6 times, and the lowest of the six stabilization energies computed in the molecular dynamics runs for each *S*-CDQ/zeolite complex was taken as the reported stabilization energy for that *S*-CDQ. The stabilization energy is the Helmholtz free energy of interaction between the *S*-CDQ and the zeolite, and it is reported per *S*-CDQ and per mol Si.

2.2. Materials Synthesis. The procedures for the preparation of OSDAs and their characterization are provided in the Supporting Information. For the synthesis of molecular sieves, the bromide (or iodide) salts of OSDAs were dissolved in distilled water and ion-exchanged to hydroxide forms using Dowex resin. The germanosilicate STW-type molecular sieves were mainly synthesized with agitation in fluoride media with a typical gel composition for CDQ2 as 1 SiO_2: x (x = 0−0.1) GeO_2: 0.5 ROH: 0.5 HF: 3 H_2O and a reaction temperature of 160 °C. The detailed synthesis procedures and characterization results are described in the Supporting Information.

2.3. Material Characterization. The ^1H and ^{13}C nuclear magnetic resonance (NMR) characterization of the OSDAs was implemented on a Bruker 400 MHz spectrometer. For the identification of the framework topology and phase purity, powder X-ray diffraction (PXRD) profiles were obtained on an X-ray diffractometer (Rigaku Miniflex II) using Cu Kα radiation (1.5410 Å wavelength). The PXRD measurement of the samples treated at various temperatures was implemented on a Rigaku SmartLab diffractometer. The morphology of particles and their elemental compositions were analyzed by scanning electron microscopy and energy dispersive spectroscopy (SEM/EDS; ZEISS 1550VP; Oxford X-mas SDD detector). All-solid-state, $^1H-^{29}Si$ cross-polarized magic-angle spinning (CP-MAS), $^1H-^{13}C$ CP-MAS, and ^{19}F MAS NMR spectroscopy experiments were conducted on a Bruker 500 MHz spectrometer using a 4 mm zirconia rotor equipped with a Kel-F cap. Thermogravimetric analysis (TGA) of the synthesized materials was implemented using an STA6000 up to 800 °C at a ramping rate of 5 °C/min unless otherwise stated. Thermal treatment experiments at varied temperatures were conducted with a ramping rate of 2 °C/min and a 60 min hold under ultrazero grade air. Calcination of the sample was implemented by a ramping rate of 2 °C/min and a hold at 120 °C for 2 h, followed by a hold at 580 °C for 6h with a ramping rate of 2 °C/min. The circular dichroism (CD) spectra were acquired on an Aviv 430 spectrometer. The microED diffraction data were collected at 80 K in a Thermo Fisher Scientific Talos Arctica transmission electron microscope. The detailed experimental and refinement procedures are described in the Supporting Information. 2-Butanol isotherm and N_2 physisorption experiments were implemented on a Quantachrome Autosorb iQ.

3. RESULTS AND DISCUSSION

The design of the chiral OSDA structure for high-silica STW was conducted based on the calculated stabilization energy.

https://doi.org/10.1021/acs.chemmater.4c01792
Chem. Mater. XXXX, XXX, XXX−XXX

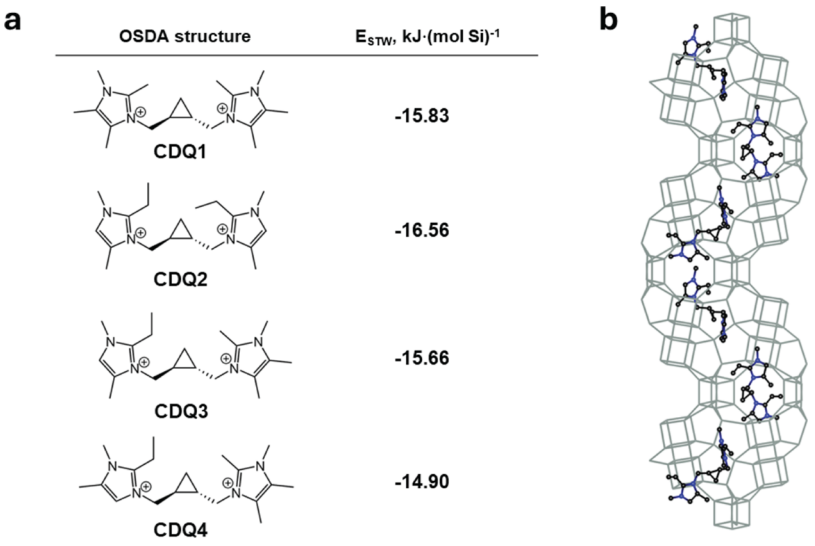

Figure 2. (a) Structures of the chiral diquaternary OSDAs and their associated stabilization energies for the STW framework. (b) STW framework occupied by a diquaternary OSDA.

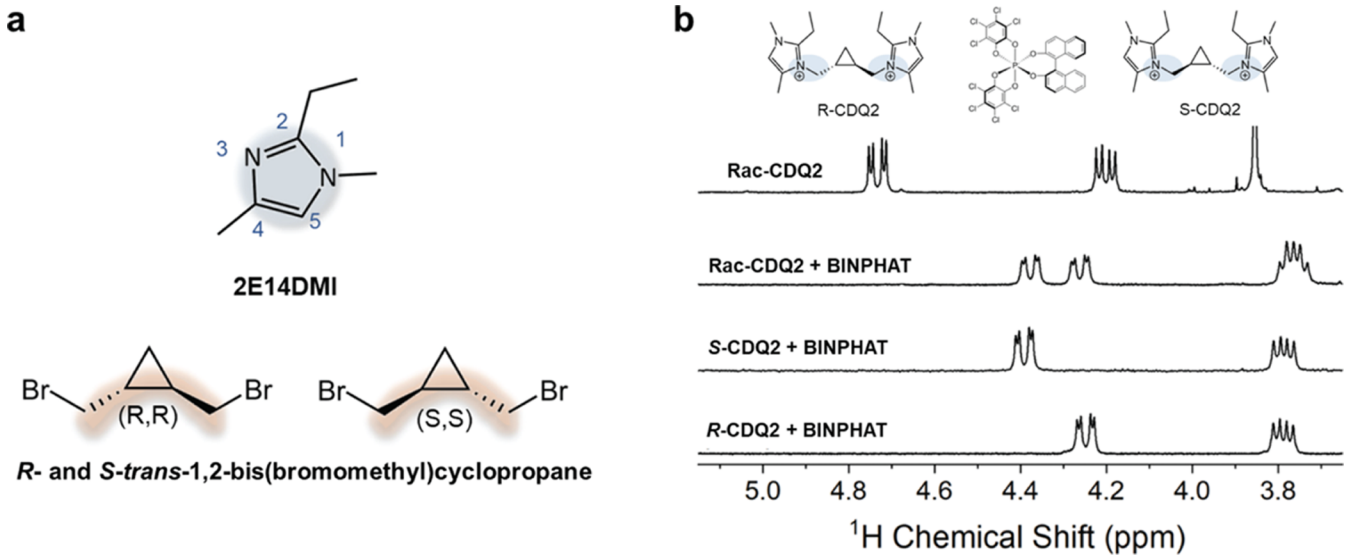

Figure 3. (a) Compounds synthesized for the preparation of CDQ2. (b) ^{1}H NMR of CDQ2 in the presence of (Λ,*R*)-BINPHAT.

The consideration of calculated stabilization energy for the crystallization of STW-type molecular sieves was initiated by Schmidt et al., where they showed that 1,2,3,4,5-pentamethylimidazolium (12345PMI) and 2-ethyl-1,3,4-trimethylimidazolium (2E134TMI) with the predicted stabilization energy of −16.5 kJ·(mol Si)$^{-1}$ successfully crystallized pure-silica STW-type molecular sieves while other alkylimidazolium OSDAs with a stabilization energy of −15.7 kJ·(mol Si)$^{-1}$ or higher did not.[19] Since the stabilization energy is calculated on the pure-silica STW framework, we hypothesized that a better (lower) stabilization energy predicted in our system would enable the higher Si content and, thus, the improved framework stability. Brand et al. reported the successful chiral OSDA that is composed of two 1,2,4,5-tetramethylimidazole (1245TMI) moieties connected by a chiral linker (CDQ1, Figure 2a). In their computational result, the chiral linker with a cyclopropyl group was selected over other candidate structures such as cyclobutane and pyrrolidine moieties based on the stabilization energy toward the STW framework.[14] Thus, we generated the candidate diquaternary OSDAs with different alkylimidazole moieties connected by the cyclopropane-based chiral linker and examined the stabilization within the STW frameworks (Figure 2).

Among various candidate structures, a symmetric chiral OSDA with a 2-ethyl-1,4-dimethylimidazole (2E14DMI) moiety (CDQ2) was found to have a superior stabilization energy of −16.56 kJ·(mol Si)$^{-1}$ toward the pure-silica STW framework (Figure 2a). The structure of CDQ2 was considered reasonable, since 2E134TMI was already proven to have a strong crystallization ability of pure-silica STW.[22] The consistent calculations on other diquaternary OSDAs provided less favorable stabilization energies than CDQ2, and 2E14DMI showed better-predicted energy than 2-ethyl-1,5-dimethylimidazole (2E15DMI) when compared within CDQ3 and CDQ4. Collectively, we determined CDQ2 as the candidate OSDA to crystallize STW-type materials with a higher Si content.

https://doi.org/10.1021/acs.chemmater.4c01792
Chem. Mater. XXXX, XXX, XXX−XXX

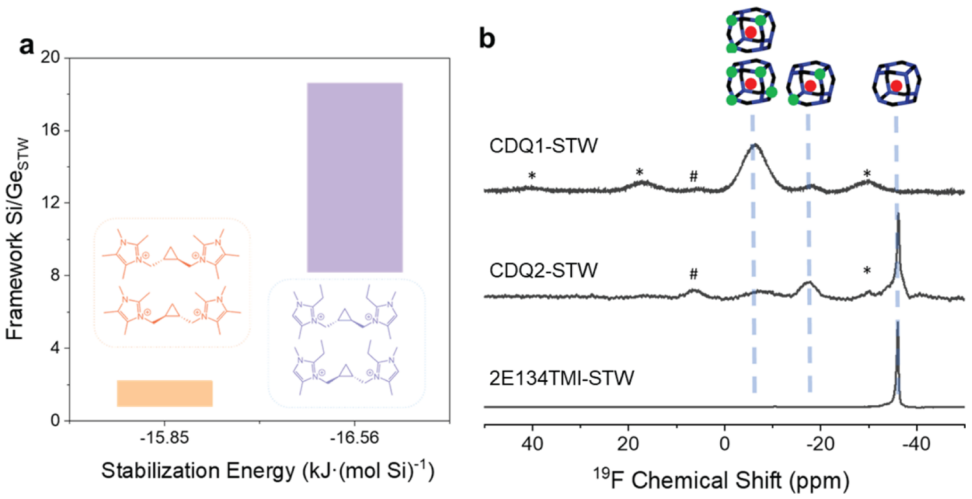

Figure 4. (a) Range of the obtained framework Si/Ge within the STW product synthesized by CDQ1 and CDQ2. The EDS results for CDQ1-STW are adopted from refs 14,24. (b) ^{19}F MAS NMR spectra of as-synthesized STW samples. * and # represent the spinning side bands.

Racemic and enantiopure forms of CDQ2 were prepared by reacting 2E14DMI with racemic and enantiopure *trans*-1,2-bis(bromomethyl)cyclopropane (Figure 3a). Since the two chiral centers exhibit the same chirality, (1*R*,2*R*)- and (1*S*,2*S*)-enantiomers are denoted *R*- and *S*-, respectively. The enantiopurity of CDQ2 was evaluated using (Λ,*R*)-BINPHAT tetrabutylammonium salt as a chiral shift reagent that induces different ^{1}H NMR chemical shifts near the ammonium groups in chiral compounds (Figure 3b).[23] The neat ^{1}H NMR spectrum of racemic and enantiopure OSDAs are identical (Figure S3). Upon addition of BINPHAT to racemic CDQ2, two equally distributed, upfield-shifted resonances between 4.2 and 4.4 ppm appear. *R*- and *S*-CDQ2 exhibit only a single resonance among these shifted peaks. Since the ratio between the split resonances provides quantitative analysis of the relative amount of two enantiomers, the absence of one of these resonances confirms the enantiopurity of *R*- and *S*-CDQ2.

The crystallization of STW-type molecular sieves using racemic, *R*-, and *S*-CDQ2 was confirmed by PXRD and SEM (Figure S4). The tested synthesis conditions and the corresponding PXRD results are summarized in Tables S1–S3. Note that the STW-type phase was obtained with the gel Si/Ge of >15, while the lower gel Si/Ge resulted in the formation of mixed phases with STW or other phases. The observed undesired phases include Beta and IWV as well as the layered (organo)silicate materials. The STW phase was more consistently obtained with a higher Si/Ge value of the gel. In the absence of Ge in the synthesis gel, no crystalline material was produced, showing that a small amount of Ge is needed to produce STW with CDQ2. The synthesis results with CDQ2 contrast with the synthesis using CDQ1, where the pure STW phase is crystallized only with a Ge-rich synthesis gel such as the gel Si/Ge of 2.

EDS analysis confirmed the high-Si composition of the STW products synthesized using CDQ2 (Figure 4a). The elemental compositions of STW-type molecular sieves obtained from CDQ1 and CDQ2 show significant differences as CDQ1 forms STW-type phases with Si/Ge between 0.8 and 2.2, whereas CDQ2 leads to the framework Si/Ge of 8.1 to 18.6. Within the gel Si/Ge range that can form pure STW phases, the product Si/Ge tends to increase as the gel Si/Ge increases. From the gel Si/Ge of 30, the Si/Ge in the product does not further increase with the gel Si/Ge (Figure S5). The framework Si/Ge of 18.6 obtained by CDQ2 is more than an 8-fold increase of Si/Ge in the STW-type material compared to CDQ1, which is consistent with our hypothesis that a better-predicted stabilization energy toward the pure-silica STW framework would lead to a higher Si content within the product.

Solid-state NMR further confirmed the increased framework Si content within the STW-type molecular sieves. The STW framework is composed of five crystallographically distinct T-sites, four of which form the d4r unit. The STW-type topology does not contain any composite building units (CBUs) other than d4r. The small d4r units impose strain within the structure due to the small angles between the consisting T atom, and Ge is preferably located within d4r due to the higher flexibility of Ge−O−Ge and Ge−O−Si bonds compared to Si−O−Si.[17] Thus, Ge has a strong structure-directing effect in the synthesis of molecular sieves containing d4r, and the need for Ge in the synthesis of enantiomerically enriched STW-type materials can also be explained in this regard. Fluoride is known as a mineralizing agent for molecular sieves with d4r based on its compactness and the covalent coordination with eight Si atoms in d4r.[18,19] Pulido et al.[20] demonstrated that the ^{19}F NMR chemical shift is influenced by the composition of Si and Ge.[14] The ^{19}F MAS NMR spectra of 2E134TMI-STW (Si/Ge = ∞), CDQ1-STW (Si/Ge = 1.2), and CDQ2-STW (Si/Ge = 18) are shown in Figure 3b. 2E134TMI-STW shows a single resonance at −36 ppm, which corresponds to the d4r with 8 Si atoms (denoted 8Si0Ge). In contrast, CDQ1-STW exhibits no resonance at −36 ppm. Instead, the resonance at −7 ppm that corresponds to 5Si3Ge and 4Si4Ge is dominant, with a small portion of the peak at around −18 ppm that corresponds to 6Si2Ge. A similar ^{19}F NMR spectrum was obtained for CDQ1-STW with a Si/Ge of 2.2.[16] Interestingly, CDQ2-STW shows a dominant resonance at −36 ppm, revealing that the material is mostly composed of pure-silica d4r. A smaller fraction of the 6Si2Ge unit is observed at −18 ppm, and the d4r unit with more Ge atoms is barely observed. The ^{29}Si CP-MAS NMR spectra also show a significant difference between CDQ1-STW and CDQ2-STW, where CDQ2-STW exhibits a much smaller resonance between −90 and −100 ppm (Figure S6). Since the formation of the

https://doi.org/10.1021/acs.chemmater.4c01792
Chem. Mater. XXXX, XXX, XXX−XXX

Si−O−Ge bond induces a downfield shift of the ^{29}Si resonance, the relative intensity of these downfield resonances is proportional to the amount of framework-incorporated Ge.[25] Thus, the significantly lower intensity of the downfield resonance found in CDQ2-STW indicates the smaller composition of framework Ge.

The lability of the Ge−O bond makes it susceptible to hydrolysis. The Ge−O−Si linkage then forms Ge−OH and HO−Si moieties. Thus, germanosilicate molecular sieves with a high Ge content exhibit low framework stability upon the removal of OSDA. As shown in Figure S7, CDQ1-STW with a framework Si/Ge of 1.2 maintains the crystal structure upon the thermal treatment at 400 °C. As the pore-filling OSDAs are removed at 500 °C and above (Table S5), the STW framework collapses and forms an amorphous phase.

The CDQ2-STW with a framework Si/Ge of 18 maintains crystallinity after thermal treatments at temperatures higher than those of CDQ1-STW (Figure 5). The change in the relative intensities of PXRD peaks upon the removal of OSDA at 600 °C is consistent with the pure-silica STW synthesized with 2E134TMI (Figure S9). The STW framework structure is maintained upon repeated thermal treatment at 800 °C. The micropore volume of calcined *R*- and *S*-CDQ2-STW (0.109−0.162 cm^3/g, Table S6) further confirms the retained pore accessibility upon the removal of OSDA. These results demonstrate the potential for a recyclable catalyst and adsorbent that can be regenerated by thermally removing the organic species occluded within the material (e.g., coke and/or adsorbates).

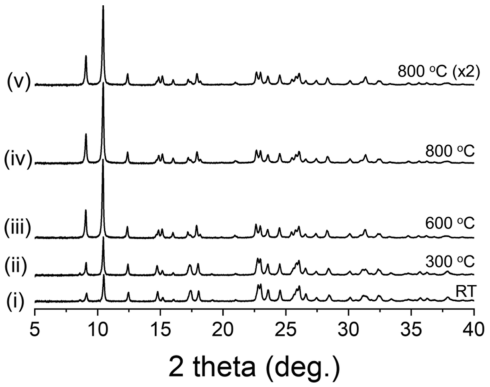

Figure 5. PXRD pattern of CDQ2-STW (Si/Ge = 18) before and after thermal treatments: (i) as-synthesized material; (ii−iv): (i) after thermal treatment at (ii) 300 °C, (iii) 600 °C, and (iv) 800 °C; and (v): (iv) after a repeated thermal treatment at 800 °C.

The STW-type molecular sieve synthesis is facilitated by the addition of fluoride in the gel, which greatly hinders mass production for commercial use due to a variety of issues. Shinno et al. demonstrated the fluoride-free synthesis of STW-type molecular sieves via a dry gel conversion (DGC) approach and the addition of Ge to the gel.[26] The synthesis was enabled by using 12345PMI, which has a strong structure-directing ability to crystallize pure-silica STW. Here, the DGC approach was employed for the fluoride-free synthesis using *S*-CDQ2. STW-type molecular sieves were successfully synthesized using *S*-CDQ2 at various conditions (Table S7; these products are denoted DGC-CDQ2-STW). The framework Si/Ge (2.1−3.3) of DGC-CDQ2-STW was lower than those of the products of fluoride-mediated synthesis, which is consistent with the results with 12345PMI, where DGC resulted in a Si/Ge of 4.3, while the fluoride-mediated synthesis can provide pure-silica STW. The crystallinity of DGC-CDQ2-STW was still partially retained after thermal treatment up to 750 °C (Figure S10), and the TGA analysis shows that about 3 OSDAs are occluded within a unit cell (Figure S11). The DGC synthesis results support the strong structure-directing ability of CDQ2 for the STW framework based on the superior stabilization energy toward the STW framework.

Since the improvement of the framework composition is associated with the use of new OSDA, it is critical to characterize CDQ2 within the crystalline product. Solid-state ^{1}H−^{13}C CP-MAS NMR spectra of as-synthesized CDQ2-STW showed that both racemic and enantiopure CDQ2 are intact within the material (Figure 6a). The TGA analysis up to 800 °C showed that ∼3 molecules of CDQ2 are occluded within a unit cell (Figure 6b). Since CDQ2 is a diquaternary OSDA with two imidazolium moieties, the OSDA occupancy is consistent with the ideal occupancy of achiral imidazolium OSDA, 6 molecules per unit cell.[19] CDQ2 contains the imidazole moiety that absorbs UV light, and the chirality of CDQ2 was characterized by CD within the UV region (Figure 6c).[27] The CDQ2 bromide salt, when pelletized with KCl, exhibits opposite polarities around 245 nm for *R*- and *S*-enantiomers. The as-synthesized *R*- and *S*-CDQ2-STW in the KCl pellet also showed the opposite polarities and their directions are consistent with the CDQ2 bromide salt. The *R*- and *S*-CDQ2-STW were then dissolved in HF, and CDQ2 was extracted in the aqueous solution. While the wavelength of the absorbed light was shifted to 230 nm in the aqueous media, the CD spectra showed consistent directions of CD signals for opposite enantiomers. These results show the retained enantioenrichment of *R*- and *S*-CDQ2 upon the hydrothermal synthesis of STW-type molecular sieves.

Previous synchrotron XPD studies have revealed the structure of *R*-CDQ1 occluded within the crystallized STW framework with the $P6_522$ space group, demonstrating the preferred fitting between the enantiopure OSDA and the corresponding STW framework.[24] Hence, the enantioenrichment of STW is indirectly proven by the retained chirality of CDQ2.[24] However, the characterization of the framework structure is still desired for the analysis of the chirality of the polycrystalline material. Unlike CDQ2, whose chirality can be characterized by spectroscopic analysis, determination of the structural chirality of the STW crystal without demonstrating the enantioselectivity in the catalytic reactions and adsorption experiments is nontrivial. We have previously reported the chirality analysis of STW crystals by 3D high-resolution transmission electron microscopy (HRTEM).[14] Since the two enantiomers of STW with $P6_122$ and $P6_522$ space groups exhibit the opposite direction of 6-fold helical rotation along the screw axis, the projection of the STW framework observed from the HRTEM shifts differently by the rotation of the crystal. Thus, by the comparison of the images aligned along $[2\bar{1}\bar{1}0]$ and $[1\bar{1}00]$ zone axes in the course of continuous tilting, the chirality of *R*- and *S*-STW crystals was determined.[28]

While single-crystal XRD is a more frequently used technique to determine the absolute stereochemistry of crystalline materials, it is not amenable to CDQ2-STW due to the small crystal size (SEM images in Figure S4). Three-dimensional microcrystal electron diffraction (microED) has been a rapidly developing technique using TEM, and it has

https://doi.org/10.1021/acs.chemmater.4c01792
Chem. Mater. XXXX, XXX, XXX−XXX

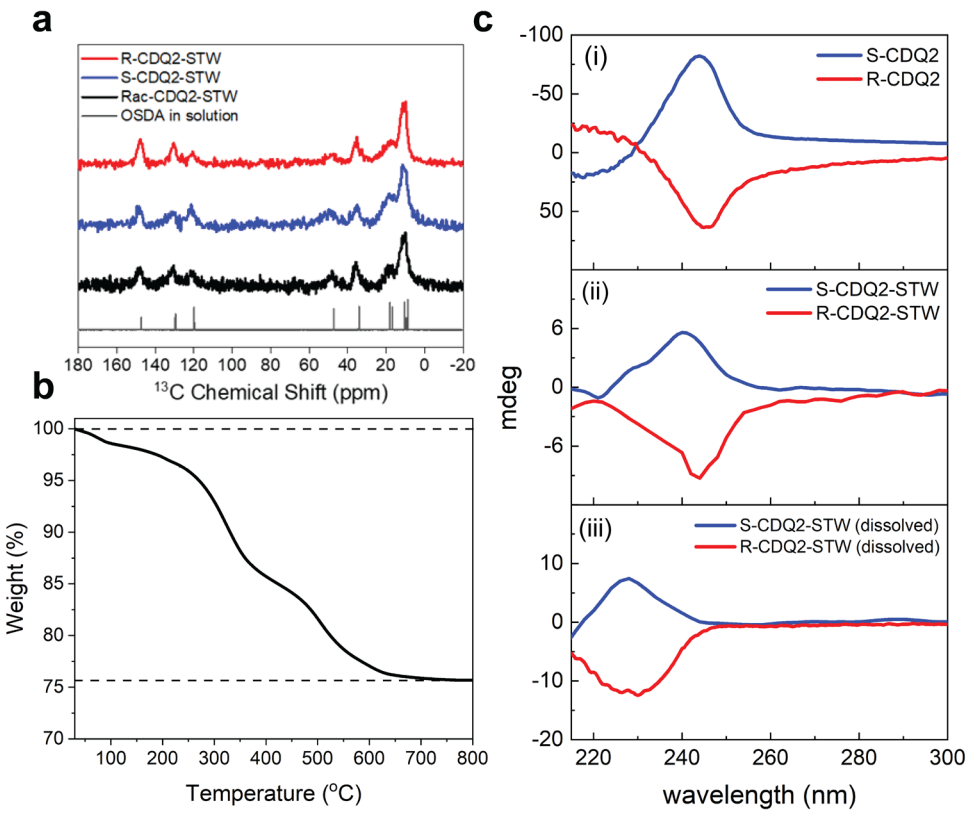

Figure 6. (a) $^{1}H-^{13}C$ CP-MAS spectra of CDQ2-STW, (b) TGA data of *S*-CDQ2-STW and (c) CD spectra of (i) CDQ2 bromide salt in a KCl pellet, (ii) as-synthesized CDQ2-STW in a KCl pellet, and (iii) CDQ2 within aqueous solution after the HF-mediated dissolution of CDQ2-STW.

been proven to be an effective tool for the crystal structure analysis of submicrometric crystals.[29] Recently, Klar et al. demonstrated the absolute structure analysis of crystalline materials by the combination of dynamical and kinematical refinements of continuous-rotation microED data.[30] The absolute structure of the as-synthesized form of a pure-silica STW-type molecular sieve, HPM-1, was determined by dynamical refinement with the $P6_122$ space group. This approach could also provide comprehensive information on the crystal structure of HPM-1 other than the chirality. Thus, we employed the continuous-rotation microED to analyze the chirality of the high-silica STW-type molecular sieve crystals in this study.

To characterize the chirality of the CDQ2-STW framework without the information on occluded OSDA, the CDQ2-STW samples were calcined before the electron diffraction measurement. The diffraction data sets were first processed with kinematical reflection to refine the crystal structure of CDQ2-STW. The crystal data and the refined structure are described in Tables S8, S9 and Figure S12. For the analysis of the absolute stereochemistry of the structure, three crystals of *R*- and *S*-CDQ2-STW were selected, and the initial crystal structure was refined against the dynamical reflection file using 10 cycles of refinement, inverted, and refined against the same dynamical reflection file using 10 refinement cycles. After the refinement with both $P6_122$ and $P6_522$, the space group with the lower residual factor was assigned for each crystal (Table S10). Figure 7 shows the wR_{all} values of the STW crystals analyzed by the dynamical refinement. *R*- and *S*-CDQ2-STW crystals are determined to be $P6_522$ and $P6_122$, respectively. Hence, the dynamical refinement of all of the

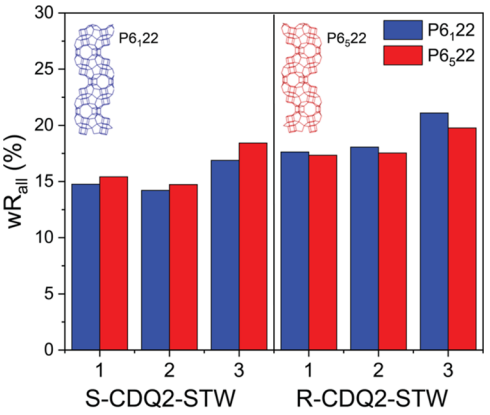

Figure 7. Summary of residual factor wR_{all} from the dynamical refinement of *R*- and *S*-CDQ2-STW crystals with $P6_122$ and $P6_522$.

diffraction data sets demonstrates the stereochemistry of the STW crystals directed by the chirality of CDQ2.

Since the STW framework shows linear chirality by the rotation of the helical pore, the key to the enantioselectivity of the STW molecular sieve is primarily based on the geometric interaction between the pore surface and the molecule that passes through the pore. To examine whether enantioenriched CDQ2-STW exhibits enantioselective behaviors, 2-butanol adsorption experiments were performed. *S*-CDQ2-STW was tested for the adsorption of racemic, (+)-, and (−)-2-butanol (Figure 8). (+)-2-Butanol is more selectively adsorbed on the *S*-CDQ2-STW compared to (−)-2-butanol, while the amount of racemic 2-butanol adsorption is between the two enantiomers. While differences in the isotherms are not large

https://doi.org/10.1021/acs.chemmater.4c01792
Chem. Mater. XXXX, XXX, XXX−XXX

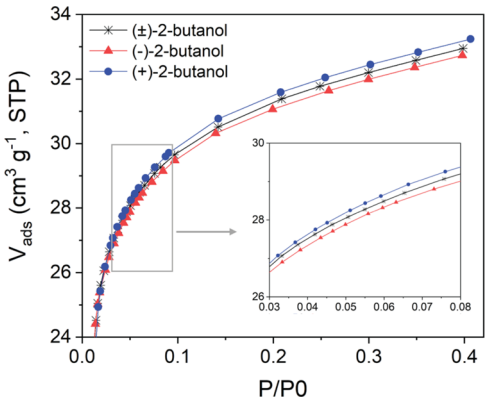

Figure 8. 2-Butanol adsorption isotherms of *S*-CDQ2-STW at 278 K.

(single separation step), they do suggest that enantiomeric separation could be possible when using columns containing the STW-type materials (as thousands of separation steps would occur with that mode of contact). Combined with the superior thermal stability that enables regeneration, the enantioselective adsorption property of CDQ2-STW demonstrates its potential as an adsorbent for chiral separations.

4. CONCLUSIONS

We prepared the enantiopure forms of a new chiral diquaternary OSDA, CDQ2, that was conceived with the aid of computational design based on the predicted stabilization energy toward STW-type framework topology. Using a fluoride-mediated hydrothermal reaction condition with a high Si content, CDQ2 crystallized the STW-type germanosilicate molecular sieves. EDS and solid-state NMR characterization confirmed the high Si/Ge ratio within the STW product framework. The high-silica STW prepared with enantiopure CDQ2 exhibits enhanced framework stability upon thermal treatment up to 800 °C. The retained structure of enantiopure CDQ2 occluded in the STW framework was characterized by solid-state NMR and CD measurements. The dynamical refinement procedure, combined with the rotational microED technique, was applied to the calcined STW samples. $P6_122$ and $P6_522$ space groups were assigned for STW crystals prepared by opposite enantiopure CDQ2, demonstrating the characterization of absolute stereochemistry of polycrystalline molecular sieves. The enantioenriched molecular sieve exhibits the enantioselective adsorption of 2-butanol. Collectively, the results in this study confirmed the rational synthesis of an enantiomerically enriched molecular sieve with the high-Si framework composition based on the stabilization energy of OSDA toward a purely siliceous framework structure.

■ ASSOCIATED CONTENT

Data Availability Statement

The raw MicroED data for the dynamical refinement in this study are available at DOI: 10.5281/zenodo.13716205.

Supporting Information

The Supporting Information is available free of charge at https://pubs.acs.org/doi/10.1021/acs.chemmater.4c01792.

Synthesis details and results; NMR analysis data; XRD profiles; SEM images; EDS results; TGA analysis results; microED details; and crystallographic information on STW-type molecular sieves (PDF)

Accession Codes

CCDC 2355978 and 2352476 contain the supplementary crystallographic data for this paper. These data can be obtained free of charge via www.ccdc.cam.ac.uk/data_request/cif, or by emailing data_request@ccdc.cam.ac.uk, or by contacting The Cambridge Crystallographic Data Centre, 12 Union Road, Cambridge CB2 1EZ, U.K.; fax: + 44−1223−336033.

■ AUTHOR INFORMATION

Corresponding Author

Mark E. Davis − *Chemical Engineering, California Institute of Technology, Pasadena, California 91125, United States;* orcid.org/0000-0001-8294-1477; Email: mdavis@cheme.caltech.edu

Authors

Youngkyu Park − *Chemical Engineering, California Institute of Technology, Pasadena, California 91125, United States;* orcid.org/0000-0001-7328-7565

Faisal H. Alshafei − *Chemical Engineering, California Institute of Technology, Pasadena, California 91125, United States; Department of Chemical Engineering, Massachusetts Institute of Technology, Cambridge, Massachusetts 02139, United States*

Lygia Silva De Moraes − *Division of Chemistry and Chemical Engineering, California Institute of Technology, Pasadena, California 91125, United States*

Isabel Hernandez Rodriguez − *Division of Chemistry and Chemical Engineering, California Institute of Technology, Pasadena, California 91125, United States*

Michael W. Deem − *SmartHealth Catalyzer, Inc., Riverwoods, Illinois 60015, United States; Certus LLC, Houston, Texas 77002, United States*

Hosea M. Nelson − *Division of Chemistry and Chemical Engineering, California Institute of Technology, Pasadena, California 91125, United States*

Complete contact information is available at: https://pubs.acs.org/10.1021/acs.chemmater.4c01792

Notes

The authors declare no competing financial interest.

■ ACKNOWLEDGMENTS

The research was supported by Chevron Energy Technology Company (Grant No. CW789506) and NSF CCI Center for Computer Assisted Synthesis (Grant No. CHE-2202693). Y.P. gratefully acknowledges Dr. Stacey I. Zones (Chevron) and Dr. Donglong Fu (Tianjin University) for their advice and discussions, Dr. Sonjong Hwang (Caltech) for his assistance with solid-state NMR data collection, Dr. Jeong Hoon Ko (MIT) for his advice in organic synthesis, Dr. Jay R. Winkler (Caltech) for assistance with the circular dichroism experiments, Dr. Jong Hun Kang (Seoul National University) for his advice, and Kwanjeong Educational Foundation for financial support. F.H.A. thanks Aramco R&D for financial support. I.H.R is supported by the NSF Graduate Research Fellowship under Grant No. 2139433.

■ REFERENCES

(1) Caldwell, J. Importance of Stereospecific Bionalytical Monitoring in Drug Development. *J. Chromatogr. A* **1996**, *719* (1), 3−13.

(2) Hutt, A. J.; Caldwell, J. The Metabolic Chiral Inversion of 2-Arylpropionic Acids - a Novel Route with Pharmacological Consequences. *J. Pharm. Pharmacol.* **2011**, *35* (11), 693−704.
(3) Ariëns, E. J. Stereochemistry: A Source of Problems in Medicinal Chemistry. *Med. Res. Rev.* **1986**, *6* (4), 451−466.
(4) Maier, N. M.; Franco, P.; Lindner, W. Separation of Enantiomers: Needs, Challenges, Perspectives. *J. Chromatogr. A* **2001**, *906* (1), 3−33.
(5) McMorn, P.; J Hutchings, G. Heterogeneous Enantioselective Catalysts: Strategies for the Immobilisation of Homogeneous Catalysts. *Chem. Soc. Rev.* **2004**, *33* (2), 108−122.
(6) Wu, C.-D.; Hu, A.; Zhang, L.; Lin, W. A Homochiral Porous Metal−Organic Framework for Highly Enantioselective Heterogeneous Asymmetric Catalysis. *J. Am. Chem. Soc.* **2005**, *127* (25), 8940−8941.
(7) Zaera, F. Chirality in Adsorption on Solid Surfaces. *Chem. Soc. Rev.* **2017**, *46* (23), 7374−7398.
(8) Davis, M. E. Zeolites and Molecular Sieves: Not Just Ordinary Catalysts. *Ind. Eng. Chem. Res.* **1991**, *30* (8), 1675−1683.
(9) Joy, A.; Ramamurthy, V. Chiral Photochemistry within Zeolites. *Chem. - Eur. J.* **2000**, *6* (8), 1287−1293.
(10) Davis, M. E. A Thirty-Year Journey to the Creation of the First Enantiomerically Enriched Molecular Sieve. *ACS Catal.* **2018**, *8* (11), 10082−10088.
(11) van Erp, T. S.; Caremans, T. P.; Dubbeldam, D.; Martin-Calvo, A.; Calero, S.; Martens, J. A. Enantioselective Adsorption in Achiral Zeolites. *Angew. Chem.* **2010**, *122* (17), 3074−3077.
(12) Sivaguru, J.; Poon, T.; Franz, R.; Jockusch, S.; Adam, W.; Turro, N. J. Stereocontrol within Confined Spaces: Enantioselective Photooxidation of Enecarbamates Inside Zeolite Supercages. *J. Am. Chem. Soc.* **2004**, *126* (35), 10816−10817.
(13) Yu, J.; Xu, R. Chiral Zeolitic Materials: Structural Insights and Synthetic Challenges. *J. Mater. Chem.* **2008**, *18* (34), 4021−4030.
(14) Brand, S. K.; Schmidt, J. E.; Deem, M. W.; Daeyaert, F.; Ma, Y.; Terasaki, O.; Orazov, M.; Davis, M. E. Enantiomerically Enriched, Polycrystalline Molecular Sieves. *Proc. Natl. Acad. Sci. U.S.A.* **2017**, *114* (20), 5101−5106.
(15) IZA-SC. Database of Zeolite Structures. http://www.iza-structure.org/databases/ (accessed March 31, 2024).
(16) de la Serna, R.; Nieto, D.; Sainz, R.; Bernardo-Maestro, B.; Mayoral, Á.; Márquez-Álvarez, C.; Pérez-Pariente, J.; Gómez-Hortigüela, L. GTM-3, an Extra-Large Pore Enantioselective Chiral Zeolitic Catalyst. *J. Am. Chem. Soc.* **2022**, *144* (18), 8249−8256.
(17) de la Serna, R.; Arnaiz, I.; Márquez-Álvarez, C.; Pérez-Pariente, J.; Gómez-Hortigüela, L. Inversion of Chirality in GTM-4 Enantio-Enriched Zeolite Driven by a Minor Change of the Structure-Directing Agent. *Chem. Commun.* **2022**, *58* (94), 13083−13086.
(18) de la Serna, R.; Jurado-Sánchez, J.; Márquez-Álvarez, C.; Pérez-Pariente, J.; Gómez-Hortigüela, L. A Chiral Zeolite Material with Improved Enantioselective Catalytic Properties Prepared from Readily Accessible Ephedrine Alkaloids. *Microporous Mesoporous Mater.* **2024**, *371*, No. 113083.
(19) Schmidt, J. E.; Deem, M. W.; Davis, M. E. Synthesis of a Specified, Silica Molecular Sieve by Using Computationally Predicted Organic Structure-Directing Agents. *Angew. Chem., Int. Ed.* **2014**, *53* (32), 8372−8374.
(20) Pulido, A.; Sastre, G.; Corma, A. Computational Study of 19F NMR Spectra of Double Four Ring-Containing Si/Ge-Zeolites. *ChemPhysChem* **2006**, *7*, 1092−1099.
(21) Pophale, R.; Daeyaert, F.; Deem, M. W. Computational Prediction of Chemically Synthesizable Organic Structure Directing Agents for Zeolites. *J. Mater. Chem. A* **2013**, *1* (23), 6750−6760.
(22) Rojas, A.; Camblor, M. A. A Pure Silica Chiral Polymorph with Helical Pores. *Angew. Chem., Int. Ed.* **2012**, *51* (16), 3854−3856.
(23) Lacour, J.; Vial, L.; Herse, C. Efficient NMR Enantiodifferentiation of Chiral Quats with BINPHAT Anion. *Org. Lett.* **2002**, *4* (8), 1351−1354.
(24) Kang, J. H.; McCusker, L. B.; Deem, M. W.; Baerlocher, C.; Davis, M. E. Further Investigations of Racemic and Chiral Molecular Sieves of the STW Topology. *Chem. Mater.* **2021**, *33* (5), 1752−1759.
(25) Rigo, R. T.; Balestra, S. R. G.; Hamad, S.; Bueno-Perez, R.; Ruiz-Salvador, A. R.; Calero, S.; Camblor, M. A. The Si−Ge Substitutional Series in the Chiral STW Zeolite Structure Type. *J. Mater. Chem. A* **2018**, *6* (31), 15110−15122.
(26) Shinno, Y.; Iyoki, K.; Ohara, K.; Yanaba, Y.; Naraki, Y.; Okubo, T.; Wakihara, T. Toward Efficient Synthesis of Chiral Zeolites: A Rational Strategy for Fluoride-Free Synthesis of STW-Type Zeolite. *Angew. Chem., Int. Ed.* **2020**, *59* (45), 20099−20103.
(27) Li, B. S.; Wen, R.; Xue, S.; Shi, L.; Tang, Z.; Wang, Z.; Tang, B. Z. Fabrication of Circular Polarized Luminescent Helical Fibers from Chiral Phenanthro[9,10]Imidazole Derivatives. *Mater. Chem. Front.* **2017**, *1* (4), 646−653.
(28) Ma, Y.; Oleynikov, P.; Terasaki, O. Electron Crystallography for Determining the Handedness of a Chiral Zeolite Nanocrystal. *Nat. Mater.* **2017**, *16* (7), 755−759.
(29) Gemmi, M.; Mugnaioli, E.; Gorelik, T. E.; Kolb, U.; Palatinus, L.; Boullay, P.; Hovmöller, S.; Abrahams, J. P. 3D Electron Diffraction: The Nanocrystallography Revolution. *ACS Cent. Sci.* **2019**, *5* (8), 1315−1329.
(30) Klar, P. B.; Krysiak, Y.; Xu, H.; Steciuk, G.; Cho, J.; Zou, X.; Palatinus, L. Accurate Structure Models and Absolute Configuration Determination Using Dynamical Effects in Continuous-Rotation 3D Electron Diffraction Data. *Nat. Chem.* **2023**, *15*, 848−855.

https://doi.org/10.1021/acs.chemmater.4c01792
Chem. Mater. XXXX, XXX, XXX−XXX